INTERNATIONAL JOURNAL OF ROBUST AND NONLINEAR CONTROL

Int. J. Robust. Nonlinear Control 2010; **00**:i–xxiii

Published online in Wiley InterScience (www.interscience.wiley.com). DOI: 10.1002/rnc

Real-time nonlinear moving horizon observer with pre-estimation for aircraft sensor fault detection and estimation †

Yiming Wan[1]*, Tamás Keviczky[2]

[1]*Massachusetts Institute of Technology, USA.*

[2]*Delft Center for Systems and Control, Delft University of Technology, The Netherlands.*

SUMMARY

This paper presents a real-time nonlinear moving horizon observer with pre-estimation and its application to aircraft sensor fault detection and estimation. A moving horizon observer determines the state estimates by minimizing the output estimation errors online, considering a finite sequence of current and past measured data and the available system model. To achieve real-time implementability of such an online optimization based observer, two particular strategies are adopted. First, a pre-estimating observer is embedded to compensate for model uncertainties, so that the calculation of disturbance estimates in a standard moving horizon observer can be avoided without losing much estimation performance. This strategy significantly reduces the online computational complexity. Second, a real-time iteration scheme is proposed by performing only one iteration of sequential quadratic programming with local Gauss-Newton approximation to the nonlinear optimization problem. Since existing stability analyses of real-time moving horizon observers cannot address the incorporation of the pre-estimating observer, a new stability analysis is performed in the presence of bounded disturbances and noises. Using a nonlinear passenger aircraft benchmark simulator, the simulation results show that the proposed approach achieves a good compromise between estimation performance and computational complexity, compared to extended Kalman filtering and two other moving horizon observers. Copyright © 2010 John Wiley & Sons, Ltd.

Received . . .

KEY WORDS: nonlinear moving horizon observer; real-time computation; fault detection; aircraft

1. INTRODUCTION

*Correspondence to: Massachusetts Institute of Technology, 77 Massachusetts Avenue, Cambridge, MA 02139, USA. E-mail: ywan@mit.edu

†Contract/grant sponsor: European Union's Seventh Framework Programme FP7/2007-2013 entitled "Reconfiguration of Control in Flight for Integral Global Upset Recovery"; contract/grant number: AAT-2012-RTD-2314544.

Model based fault detection (FD) and estimation is recognized as a promising technique to facilitate the automated handling of abnormal events, e.g., in aerospace applications [1, 2]. To deal with a wide range of operating points, it is necessary to adopt nonlinear observer or filtering approaches to detect faults and provide reliable state or fault estimates. Based on the types of adopted models, these approaches can be classified as (i) a direct nonlinear model-based design including nonlinear geometric observers [3], high-gain observers [4, 5], sliding mode observers [6, 7], and nonlinear Kalman filtering [8–11]; and (ii) a linear parameter varying (LPV) model-based design using a LPV approximation to the nonlinear system [12–15]. In these approaches, except the nonlinear Kalman filtering, the observer or filter parameters are designed offline. Their design methodologies are often restricted to certain class of nonlinear systems, or not applicable to high nonlinearity.

In contrast to the above observers or filters with fixed parameters designed offline, the moving horizon observer (MHO) is based on online optimization [16, 17]. It is also referred to as moving horizon estimation when inequality constraints are incorporated [18, 19]. The MHO estimates states and process disturbances by minimizing the difference between its estimates and data samples within a finite past horizon. The extended Kalman filter (EKF) can be viewed as a special form of MHO with its moving horizon length set to 1. Compared to EKF, the MHO achieves better performance in terms of estimation accuracy and robustness to initial errors due to utilizing a batch of past measured samples at each time instant [20]. It relies on numerical optimization as a systematic approach to address various nonlinearities and constraints [21, 22]. Moreover, it is able to cope with non-uniform observability, time-varying systems, and unknown parameters, which are often troublesome for conventional observer designs [23–25]. Recently, the MHO has received attention in different aerospace applications [26–30].

Despite its benefits, the computational burden of online optimization in MHO is a critical challenge that limits its applicability in real time, especially for fast nonlinear dynamic systems such as in aircraft applications. To speedup computation, many efficient computation strategies have been reported in the literature [21]. In [31], a structure-exploiting Riccati-based approach was proposed by following the similar approach in model predictive control, so that the computational complexity is linear with respect to the horizon length. In [32], the computation is accelerated by exploiting sensitivity analysis of a background MHO solution. Even with such efficient algorithms, in order to be compliant with a short sampling interval, only a limited number of iterations are allowed, thus the optimization problem at each time instant cannot be fully solved. As a consequence, the established stability analysis for MHOs with fully solved optimizations in [18, 33] cannot be applied to such real-time iteration schemes. For real-time MHO using gradient, conjugate gradient, and Newton methods, different types of stability analyses have been proposed in [22, 34].

Motivated by the idea of pre-stabilizing model predictive control, a new linear MHO was proposed in [35, 36] by incorporating a pre-estimating observer for forward prediction. While model

DOI: 10.1002/rnc

uncertainties in forward prediction are compensated for by disturbance estimates in a standard MHO formulation [18], this is achieved by feedback injection from output measurements in an MHO with pre-estimation (MHO-PE). By avoiding the explicit calculation of disturbance estimates, the MHO-PE has a computational complexity that scales significantly better with respect to the horizon length and the disturbance dimensions, compared to the standard MHO. This idea has been recently extended to nonlinear systems in [37, 38].

The above results on the MHO-PE all make use of exact solutions of the underlying optimization problem which might not be computed within a short sampling interval. Hence their real-time applicability is significantly limited. To address this issue, a real-time iteration scheme is proposed and analyzed in this paper for the nonlinear MHO-PE. It is based on sequential quadratic programming (SQP) with local Gauss-Newton approximations. During each sampling interval, only one SQP iteration is performed so that the computational cost per sample is minimized and fixed for real-time computation. The stability of estimation errors is analyzed by deriving explicit error dynamics and an upper-bounding sequence on the estimation errors. This leads to useful insights about parameter tuning in the MHO-PE for trade-offs between stability and performance. The proposed real-time MHO-PE scheme is applied to aircraft angle-of-attack (AOA) fault detection and estimation by using an aerodynamic-independent model. As shown in simulation results from a nonlinear passenger aircraft simulator [1], the proposed method achieves a good compromise between estimation performance and computational complexity, compared to two other MHO formulations.

This paper is organized as follows. In Section 2, three MHO formulations and their associated real-time computation issues are briefly reviewed. Our real-time iteration scheme for the nonlinear MHO-PE and its stability is proposed in Section 3 and analyzed in Section 4, respectively. In Section 5, a comparative simulation study using a nonlinear passenger aircraft benchmark simulator is presented.

2. PROBLEM STATEMENT AND PRELIMINARIES

Consider a nonlinear discrete-time system

$$\begin{aligned} x_{k+1} &= f(x_k, u_{m,k}) + w_k \\ y_{m,k} &= h(x_k) + v_k, \end{aligned} \tag{1}$$

where $x_k \in \mathbb{R}^{n_x}$ is the state, $u_{m,k} \in \mathbb{R}^{n_u}$ and $y_{m,k} \in \mathbb{R}^{n_y}$ are the measured system input and output, w_k and v_k are the process noise and measurement noise. For the above system model (1), the following assumptions are made:

Prepared using rncauth.cls
DOI: 10.1002/rnc

Assumption 1. The discrete-time state x, system input u, process disturbance w, and measurement noise v belong to bounded sets $\mathbb{X} \subset \mathbb{R}^{n_x}$, $\mathbb{U} \subset \mathbb{R}^{n_u}$ $\mathbb{W} \subset \mathbb{R}^{n_w}$, and $\mathbb{V} \subset \mathbb{R}^{n_v}$, respectively.

Assumption 2. The nonlinear functions $f(x,u)$ and $h(x)$ are Lipschitz with respect to $x \in \mathbb{X}$ and $u \in \mathbb{U}$.

In order to monitor the sensor that measures one entry of the state vector x_k, the system state is first estimated from the available system input $u_{m,k}$ and output $y_{m,k}$. Then the difference between the sensor measurement and its associated estimate is used to indicate the occurrence of sensor faults. This paper aims at proposing a real-time iteration scheme for the nonlinear MHO-PE to account for the hard real-time constraint, and illustrating its application to aircraft AOA sensor fault detection and estimation.

2.1. Preliminaries on nonlinear moving horizon observer

Next, three formulations of nonlinear MHO and the existing results on their real-time computation strategies are briefly reviewed.

For a moving horizon $[k-N,k]$ at each time instant k, given the a priori estimate $\bar{x}_{k-N|k}$ for the initial state x_{k-N} as well as the available input and output data $\mathcal{I}_k = \{y_{m,k-N},\cdots,y_{m,k},u_{m,k-N},\cdots,u_{m,k-1}\}$, the MHO estimates the state sequence x_{k-N}, $\cdots$, x_k by solving a nonlinear least-squares (NLS) problem in the form [18]

$$\begin{aligned}\min_{\hat{x}_{i|k},\hat{w}_{i|k}} \ & \left\|\hat{x}_{k-N|k}-\bar{x}_{k-N|k}\right\|_M^2+\sum_{i=k-N}^{k-1}\left\|\hat{w}_{i|k}\right\|_Q^2+\sum_{i=k-N}^{k}\left\|y_{m,i}-\hat{y}_{i|k}\right\|_W^2 \\ \text{s.t. } & \hat{x}_{i+1|k}=f(\hat{x}_{i|k},u_{m,i})+\hat{w}_{i|k},\ i=k-N,\cdots,k-1, \\ & \hat{y}_{i|k}=h(\hat{x}_{i|k}),\ i=k-N,\cdots,k,\end{aligned} \tag{2}$$

where $\hat{x}_{i|k}$ and $\hat{y}_{i|k}$ represent the estimated state and output for x_i and y_i using the information $\mathcal{I}_k$ at time instant k. The first term of the objective function in (2) is the so-called arrival cost to account for data before the current estimation horizon. The positive definite matrices M, Q, and W are tuning parameters for trade-offs between different components of the objective function. At each time instant k, a typical MHO algorithm involves three steps:

(i) Update and initialization using estimates $\{\hat{x}^\star_{i|k-1},\hat{w}^\star_{i|k-1}\}$ obtained over the previous horizon $[k-N-1,k-1]$. The a priori estimate $\bar{x}_{k-N|k}$ in the arrival-cost term is updated as $\bar{x}_{k-N|k}=\hat{x}^\star_{k-N|k-1}$ by following [33]. The initial guess of the state $\hat{x}_{k-N|k}$ and the disturbance sequence $\hat{w}_{k-N|k},\cdots,\hat{w}_{k-1|k},\hat{w}_{k|k}$ is assigned to be $\hat{x}^\star_{k-N|k-1}$ and $\hat{w}^\star_{k-N|k-1},\cdots,\hat{w}^\star_{k-1|k-1},0$, respectively.

(ii) Optimization. By eliminating the state variables $\hat{x}_{k-N+1|k},\cdots,\hat{x}_{k|k}$ using the dynamic equations in the constraints of (2), the problem (2) turns into a condensed form $J_k(\hat{x}_{k-N|k},\hat{w}_{k-1|k}^{k-N})$ with respect to the state $\hat{x}_{k-N|k}$ and the disturbance sequence $\hat{w}_{k-1|k}^{k-N}=$

Prepared using rncauth.cls
DOI: 10.1002/rnc

$\begin{bmatrix}\hat{w}_{k-N|k}^{\mathsf{T}} & \hat{w}_{k-N+1|k}^{\mathsf{T}} & \cdots & \hat{w}_{k-1|k}^{\mathsf{T}}\end{bmatrix}^{\mathsf{T}}$. Starting from the above initial guess, the numerical optimization algorithm iteratively computes the estimates $\hat{x}^{\star}_{k-N|k}$ and $\hat{w}^{\star}_{k-N|k}, \cdots, \hat{w}^{\star}_{k-1|k}$.

(iii) Forward prediction. The remaining state estimates are computed by forward prediction from $\hat{x}^{\star}_{k-N|k}$ using $\hat{x}^{\star}_{i+1|k} = f(\hat{x}^{\star}_{i|k}, u_{m,i}) + w^{\star}_{i|k}$, $i = k-N, \cdots, k-1$.

The above step (i) is computationally cheap. Note that there are other computationally demanding alternatives such as in [19] for recursively updating the weighting matrix M, which are not suitable for the fast real-time application in this paper. In Step (ii), the computational complexity of solving the KKT system associated with the condensed formulation is $O(N^3(n_x+n_w)^3)$.

In [22, 33], another MHO formulation is also adopted without estimating the disturbances $\{w_i\}$:

$$\begin{aligned}\min_{\hat{x}_{i|k}} \; & J_k(\hat{x}_{k-N|k}) = \left\|\hat{x}_{k-N|k} - \bar{x}_{k-N|k}\right\|_M^2 + \sum_{i=k-N}^{k} \left\|y_{m,i} - \hat{y}_{i|k}\right\|_W^2 \\ \text{s.t.} \; & \hat{x}_{i+1|k} = f(\hat{x}_{i|k}, u_{m,i}),\ i = k-N, \cdots, k-1, \\ & \hat{y}_{i|k} = h(\hat{x}_{i|k}),\ i = k-N, \cdots, k.\end{aligned} \tag{3}$$

The algorithm for this MHO formulation (3) still follows the same three steps mentioned above, with two main differences. The first difference is that the condensed problem derived from (3) has only decision variable $\hat{x}_{k-N|k}$, after eliminating $\hat{x}_{k-N+1|k}, \cdots, \hat{x}_{k|k}$. Thus its computational complexity in solving the associated KKT system is $O(n_x^3)$, which does not depend on the horizon length N. Despite this computational advantage, its estimation performance can be worse than the MHO formulation (2), because its estimation errors accumulate in the forward prediction $\hat{x}_{i+1|k} = f(\hat{x}_{i|k}, u_{m,i})$ adopted in (3), especially when the dynamics $\hat{x}_{i+1|k} = f(\hat{x}_{i|k}, u_{m,i})$ is unstable and the horizon length N is large.

By introducing a nonlinear Luenberger observer into the MHO formulation (3), the MHO with pre-estimation (MHO-PE) was first proposed for linear systems [35, 36], and has been recently extended to nonlinear systems in [37, 38]:

$$\begin{aligned}\min_{\hat{x}_{i|k}} \; & J_k(\hat{x}_{k-N|k}) = \left\|\hat{x}_{k-N|k} - \bar{x}_{k-N|k}\right\|_M^2 + \sum_{i=k-N}^{k} \left\|y_{m,i} - \hat{y}_{i|k}\right\|_W^2 \\ \text{s.t.} \; & \hat{x}_{i+1|k} = f(\hat{x}_{i|k}, u_{m,i}) + L(y_{m,i} - \hat{y}_{i|k}),\ i = k-N, \cdots, k-1, \\ & \hat{y}_{i|k} = h(\hat{x}_{i|k}),\ i = k-N, \cdots, k.\end{aligned} \tag{4}$$

On one hand, the pre-estimating Luenberger observer stabilizes the forward prediction by introducing feedback from output measurements, thus reducing the error accumulation in the forward prediction. On the other hand, the observer gain L can be regarded as a parsimonious parameterization of the estimated disturbance sequence $\hat{w}_{k-N|k}$, $\cdots$, $\hat{w}_{k-1|k}$ in the MHO formulation (2), i.e., $\hat{w}_{i|k} = L(y_i - \hat{y}_{i|k})$, $i = k-N, \cdots, k-1$. Therefore, it can be expected that the estimation performance of the MHO formulation (4) can better approximate the formulation

Prepared using rncauth.cls
DOI: 10.1002/rnc

(2) than the formulation (3). The observer gain L are designed offline to stabilize the observer error dynamics by following any nonlinear Luenberger observer design procedure, e.g., [39]. By doing so, the MHO-PE formulation (4) retains the same computational advantage of the formulation (3), i.e., its computational complexity is much less dependent upon the horizon length than the formulation (2).

In real-time applications, each involved optimization problem per sample in MHO may not be full solved within a restricted sampling interval. Instead, the number of iterations per sample has to be fixed, which achieves real-time computation at the cost of losing optimality. As a consequence, the established stability analysis for MHOs with fully solved optimizations in [18, 33] cannot be applied to such real-time iteration scheme. Existing stability results for real-time MHOs with fixed number of iterations are limited to the formulation (3), see [22, 34, 40].

Remark 1

The condensed form is adopted in this paper for the three MHO formulations (2)–(4) by eliminating state variables via forward prediction. Alternatively, all state variables can be kept as optimization variables, which is known as the multiple shooting method. Such multiple shooting has been applied in [31] and [34] to solve (2) and (3), respectively. This results in a sparsely structured KKT system which is numerically better conditioned than the condensed form [34]. The multiple shooting method can be also applied to the MHO-PE (4), with the benefit of reducing computational complexity by avoiding explicit disturbance estimation compared to (2). However, the stability analysis of MHO-PE in the context of multiple shooting cannot easily follow what we have performed for the condensed MHO-PE in Section 4, which remains an open-problem for future research.

3. REAL-TIME NONLINEAR MOVING HORIZON OBSERVER WITH PRE-ESTIMATION

As discussed in Section 2.1, the MHO-PE achieves a good compromise between estimation performance and computational efficiency, compared to other two MHO formulations. For this reason, we adopt the MHO-PE method to solve the real-time nonlinear FD and estimation problem stated in Section 2. In contrast to the MHO-PE with fully solved optimizations in [36, 38], we propose a real-time iteration scheme in this section to implement the nonlinear MHO-PE, and analyze its stability in Section 4.

The proposed real-time iteration scheme is based on SQP with local Gauss-Newton approximations to the nonlinear problem (4). During each sampling interval, only one SQP iteration

DOI: 10.1002/rnc

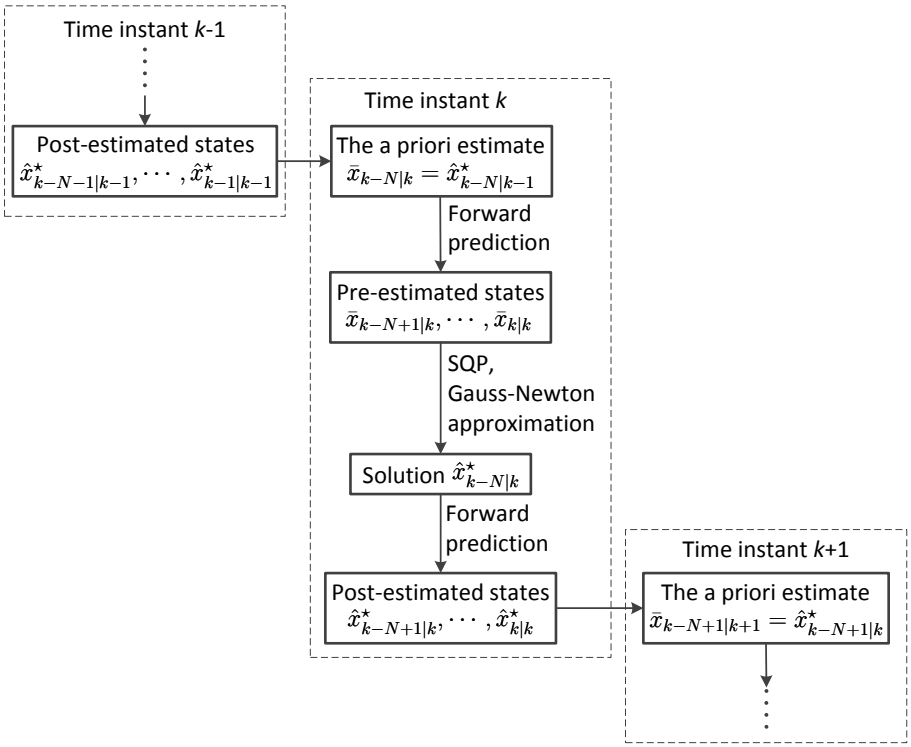

Figure 1. Block diagram of proposed real-time MHO-PE algorithm.

is performed so that the computational cost per sample is minimized and fixed for real-time computation. The algorithm is depicted in Figure 1 and described below.

Algorithm 1 (Real-time iteration for MHO-PE at each time instant k)

(i) Update and initialization using estimates $\{\hat{x}^\star_{i|k-1}, \hat{w}^\star_{i|k-1}\}$ obtained over the previous horizon $[k-N-1, k-1]$. The a priori estimate $\bar{x}_{k-N|k}$ in the arrival-cost term is updated as $\bar{x}_{k-N|k} = \hat{x}^\star_{k-N|k-1}$. The initial guess of the state $\hat{x}_{k-N|k}$ and the disturbance sequence $\hat{w}_{k-N|k}, \cdots, \hat{w}_{k-1|k}, \hat{w}_{k|k}$ is assigned to be $\hat{x}^\star_{k-N|k-1}$ and $\hat{w}^\star_{k-N|k-1}, \cdots, \hat{w}^\star_{k-1|k-1}, 0$, respectively.

(ii) One SQP iteration.

ii-1) Deriving a local Gauss-Newton approximation to the NLS problem (4):

Starting from the a priori estimate $\bar{x}_{k-N|k}$, compute the pre-estimated state sequence $\bar{x}_{k-N|k}, \bar{x}_{k-N+1|k}, \cdots, \bar{x}_{k|k}$ by

$$\bar{x}_{i+1|k} = f(\bar{x}_{i|k}, u_{m,i}) + L(y_{m,i} - h(\bar{x}_{i|k})), i = k-N, \cdots, k-1, \tag{5}$$

using the available measurements $y_{m,k-N}, \cdots, y_{m,k}, u_{m,k-N}, \cdots, u_{m,k-1}$ and the Luenberger observer embedded in (4). Then, along this pre-estimated state sequence,

Prepared using rncauth.cls
DOI: 10.1002/rnc

linearize the constraints in (4) as

$$\begin{aligned}\hat{x}_{i+1|k} &= f(\bar{x}_{i|k}, u_{m,i}) + A_{i|k}(\hat{x}_{i|k} - \bar{x}_{i|k}) + L(y_{m,i} - \hat{y}_{i|k}) \\ &= \Phi_{i|k}\hat{x}_{i|k} + Ly_{m,i} + \mu_{i|k} - L\tau_{i|k} \\ \hat{y}_{i|k} &= h(\bar{x}_{i|k}) + C_{i|k}(\hat{x}_{i|k} - \bar{x}_{i|k}) = C_{i|k}\hat{x}_{i|k} + \tau_{i|k}\end{aligned} \tag{6}$$

with $A_{i|k} = \nabla_x f(\bar{x}_{i|t}, u_{m,i})$, $C_{i|k} = \nabla_x h(\bar{x}_{i|t})$, and

$$\Phi_{i|k} = A_{i|k} - LC_{i|k},\ \mu_{i|k} = f(\bar{x}_{i|k}, u_{m,i}) - A_{i|k}\bar{x}_{i|k},\ \tau_{i|k} = h(\bar{x}_{i|k}) - C_{i|k}\bar{x}_{i|k}. \tag{7}$$

It then follows that

$$y_{m,k}^{k-N} - \hat{y}_{k|k}^{k-N} = \sigma_k - \mathcal{F}_k\hat{x}_{k-N|k},\ \sigma_k = \mathcal{H}_k y_k^{k-N} - \mathcal{G}_k\mu_{k|k}^{k-N} - \mathcal{H}_k\tau_{k|k}^{k-N}, \tag{8}$$

where $y_{m,k}^{k-N} = \begin{bmatrix} y_{m,k-N}^{\mathsf{T}} & y_{m,k-N+1}^{\mathsf{T}} & \cdots & y_{m,k}^{\mathsf{T}} \end{bmatrix}^{\mathsf{T}}$, $\hat{y}_{k|k}^{k-N}$, $\mu_{k|k}^{k-N}$, and $\tau_{k|k}^{k-N}$ are defined similarly as $\hat{y}_{k|k}^{k-N} = \begin{bmatrix} \hat{y}_{k-N|k}^{\mathsf{T}} & \hat{y}_{k-N+1|k}^{\mathsf{T}} & \cdots & \hat{y}_{k|k}^{\mathsf{T}} \end{bmatrix}^{\mathsf{T}}$,

$$\mathcal{F}_k = \begin{bmatrix} C_{k-N|k} \\ C_{k-N+1|k}\Phi_{k-N|k} \\ \vdots \\ C_{k|k}\prod_{j=k-N}^{k-1}\Phi_{j|k} \end{bmatrix},\ \mathcal{G}_k = \begin{bmatrix} 0 & 0 & \cdots & 0 \\ C_{k-N+1|k} & 0 & \cdots & 0 \\ \vdots & \vdots & \ddots & \vdots \\ C_{k|k}\prod_{j=k-N+1}^{k-1}\Phi_{j|k} & C_{k|k}\prod_{j=k-N+2}^{k-1}\Phi_{j|k} & \cdots & 0 \end{bmatrix},$$

$$\mathcal{H}_k = \begin{bmatrix} I & 0 & \cdots & 0 \\ -C_{k-N+1|k}L & I & \cdots & 0 \\ \vdots & \vdots & \ddots & \vdots \\ -C_{k|k}\prod_{j=k-N+1}^{k-1}\Phi_{j|k}L & -C_{k|k}\prod_{j=k-N+2}^{k-1}\Phi_{j|k}L & \cdots & I \end{bmatrix}. \tag{9}$$

The local Gauss-Newton approximation to the nonlinear problem (4) is a QP subproblem

$$\begin{aligned}\min_{\hat{x}_{i|k}}\ & \left\|\hat{x}_{k-N|k} - \bar{x}_{k-N|k}\right\|_M^2 + \sum_{i=k-N}^{k}\left\|y_{m,i} - \hat{y}_{i|k}\right\|_W^2 \\ \text{s.t. }& (6),\end{aligned} \tag{10}$$

By using (8), $\hat{x}_{k-N+1|k}, \cdots, \hat{x}_{k|k}$ is eliminated, and the QP subproblem (10) is transformed into the following condensed form with no constraints:

$$\begin{aligned}\min_{p_k}\ J_k^1(p_k) &= \left\|\hat{x}_{k-N|k} - \bar{x}_{k-N|k}\right\|_M^2 + \left\|y_{m,k}^{k-N} - \hat{y}_{k|k}^{k-N}\right\|_{\bar{W}}^2 \\ &= \|p_k\|_M^2 + \left\|\sigma_k - \mathcal{F}_k\bar{x}_{k-N|k} - \mathcal{F}_k p_k\right\|_{\bar{W}}^2\end{aligned} \tag{11}$$

where $\bar{W} = \mathrm{diag}(W, W, \cdots, W)$ represents a block-diagonal matrix, and $p_k = \hat{x}_{k-N|k} - \bar{x}_{k-N|k}$ is the search direction to be determined.

DOI: 10.1002/rnc

ii-2) Solving the QP subproblem (11):

The optimal search direction is

$$p_k^\star = (M + \mathcal{F}_k^\mathsf{T} \bar{W} \mathcal{F}_k)^{-1} \mathcal{F}_k^\mathsf{T} \bar{W} (\sigma_k - \mathcal{F}_k \bar{x}_{k-N|k}). \tag{12}$$

Then, the state estimate $\hat{x}^\star_{k-N|k}$ is updated as

$$\hat{x}^\star_{k-N|k} = \bar{x}_{k-N|k} + \alpha_k p_k^\star, \tag{13}$$

where the step length $\alpha_k \in (0, 1]$ is determined by a conventional backtracking line search strategy, e.g., Algorithm 3.1 in [41].

(iii) Forward prediction. Starting from $\hat{x}^\star_{k-N|k}$, compute the post-estimated state sequence $\hat{x}^\star_{k-N+1|k}, \cdots, \hat{x}^\star_{k|k}$ by

$$\hat{x}^\star_{i+1|k} = f(\hat{x}^\star_{i|k}, u_{m,i}) + L(y_{m,i} - h(\hat{x}^\star_{i|k})), i = k - N, \cdots, k. \tag{14}$$

4. STABILITY ANALYSIS

In this section, stability analysis of estimation errors of Algorithm 1 is performed by deriving explicit error dynamics and an upper-bounding sequence on the estimation errors. Such analysis allows developing useful insights on parameter tuning for trade-offs between stability and estimation performance.

Similarly to the linear MHO-PE in [35, 36], the stability of our proposed real-time nonlinear MHO-PE is characterized by the dynamics of the post-estimation error

$$e_{k-N} = x_{k-N} - \hat{x}^\star_{k-N|k}, \tag{15}$$

where $\hat{x}^\star_{k-N|k}$ is obtained after one SQP iteration in Step (ii-2) of Algorithm 1. In order to derive error dynamics for (15), the other error dynamics involved in Algorithm 1 are first introduced as follows.

- In Step (ii-1) of Algorithm 1, error dynamics between the true states x_i and the pre-estimated states $\bar{x}_{i|k}$:

  Combining (1) and (5) gives

  $$x_{i+1} - \bar{x}_{i+1|k} = f(x_i, u_{m,i}) - f(\bar{x}_{i|k}, u_{m,i}) - L(h(x_i) - h(\bar{x}_{i|k})) + w_i - Lv_i, \tag{16}$$

  According to Lemmas 6 and 7 in [39], there exist two matrices $A(x_i, \bar{x}_{i|k}, u_{m,i})$ and $C(x_i, \bar{x}_{i|k})$ with multivariate functions as their entries, such that $f(x_i, u_{m,i}) - f(\bar{x}_{i|k}, u_{m,i}) = A(x_i, \bar{x}_{i|k}, u_{m,i})(x_i - \bar{x}_{i|k})$ and $h(x_i) - h(\bar{x}_{i|k}) = C(x_i, \bar{x}_{i|k})(x_i - \bar{x}_{i|k})$ hold. Let $\bar{A}_{i,k}$, $\bar{C}_{i,k}$, and $\bar{\Xi}_{i,k}$ denote $A(x_i, \bar{x}_{i|k}, u_{m,i})$, $C(x_i, \bar{x}_{i|k})$, and $\bar{A}_{i,k} - L\bar{C}_{i,k}$, respectively. Then the error

Prepared using rncauth.cls
DOI: 10.1002/rnc

dynamics (16) can be rewritten as

$$x_{i+1} - \bar{x}_{i+1|k} = (\bar{A}_{i,k} - L\bar{C}_{i,k})(x_i - \bar{x}_{i|k}) + w_i - Lv_i = \bar{\Xi}_{i,k}(x_i - \bar{x}_{i|k}) + w_i - Lv_i. \quad (17)$$

- In Step (iii) of Algorithm 1, error dynamics between the true state x_i and the post-estimated states $\hat{x}^\star_{i|k}$:
  Similarly to (16) and (17), the dynamics of the error $x_i - \hat{x}^\star_{i|k}$ is

$$x_{i+1} - \hat{x}^\star_{i+1|k} = (\hat{A}_{i,k} - L\hat{C}_{i,k})(x_i - \hat{x}^\star_{i|k}) + w_i - Lv_i = \hat{\Xi}_{i,k}(x_i - \hat{x}^\star_{i|k}) + w_i - Lv_i, \quad (18)$$

  where $\hat{A}_{i,k}$, $\hat{C}_{i,k}$, and $\hat{\Xi}_{i,k} = \hat{A}_{i,k} - L\hat{C}_{i,k}$ are defined similarly to $\bar{A}_{i,k}$, $\bar{C}_{i,k}$, and $\bar{\Xi}_{i,k}$ in (17), respectively: $\hat{A}_{i,k}$ satisfies $f(x_i, u_{m,i}) - f(\hat{x}^\star_{i|k}, u_{m,i}) = \hat{A}_{i,k}(x_i - \hat{x}^\star_{i|k})$, and $\hat{C}_{i,k}$ satisfies $h(x_i) - h(\hat{x}^\star_{i|k}) = \hat{C}_{i,k}(x_i - \hat{x}^\star_{i|k})$. Note that the error dynamics in (17) and (18) corresponds to the forward prediction within the current horizon $[k-N, k]$, while the error dynamics for e_{k-N} in (15) aims at describing how e_{k-N} varies between successive horizons.
- Error dynamics between the pre-estimated states $\bar{x}_{i|k}$ and post-estimated states $\hat{x}^\star_{i|k}$.
  From (5) and (14), the dynamics of the error $\hat{x}^\star_{i|k} - \bar{x}_{i|k}$ is derived as

$$\hat{x}^\star_{i+1|k} - \bar{x}_{i+1|k} = (\breve{A}_{i,k} - L\breve{C}_{i,k})(\hat{x}^\star_{i|k} - \bar{x}_{i|k}) = \breve{\Xi}_{i,k}(\hat{x}^\star_{i|k} - \bar{x}_{i|k}) \quad (19)$$

  where $\breve{A}_{i,k}$, $\breve{C}_{i,k}$, and $\breve{\Xi}_{i,k} = \breve{A}_{i,k} - L\breve{C}_{i,k}$ are defined similarly to $\bar{A}_{i,k}$, $\bar{C}_{i,k}$, and $\bar{\Xi}_{i,k}$ in (17), respectively: $\breve{A}_{i,k}$ satisfies $f(\hat{x}^\star_{i|k}, u_{m,i}) - f(\bar{x}_{i|k}, u_{m,i}) = \breve{A}_{i,k}(\hat{x}^\star_{i|k} - \bar{x}_{i|k})$, and $\breve{C}_{i,k}$ satisfies $h(\hat{x}^\star_{i|k}) - h(\bar{x}_{i|k}) = \breve{C}_{i,k}(\hat{x}^\star_{i|k} - \bar{x}_{i|k})$.

4.1. Error dynamics of state estimates

With (12) and (13), the estimation error e_{k-N} in (15) can be written as

$$e_{k-N} = x_{k-N} - \bar{x}_{k-N|k} - \alpha_k(M + \mathcal{F}_k^\mathsf{T}\bar{W}\mathcal{F}_k)^{-1}\mathcal{F}_k^\mathsf{T}\bar{W}(\sigma_k - \mathcal{F}_k\bar{x}_{k-N|k}). \quad (20)$$

Then we follow two steps to derive the error dynamics of e_{k-N}: (i) express how σ_k defined in (8) is related to x_{k-N}; and (ii) express $x_{k-N} - \bar{x}_{k-N|k}$ by using the estimation error $e_{k-N-1} = x_{k-N-1} - \hat{x}^\star_{k-N-1|k-1}$ of the last horizon.

First, the system dynamics (1) is rewritten as

$$\begin{aligned} x_{i+1} &= f(\bar{x}_{i|k}, u_{m,i}) + A_{i|k}(x_i - \bar{x}_{i|k}) + \psi_f(x_i, \bar{x}_{i|k}, u_{m,i}) + w_i \\ &= A_{i|k}x_i + \mu_{i|k} + \psi_f(x_i, \bar{x}_{i|k}, u_{m,i}) + w_i \\ y_{m,i} &= h(\bar{x}_{i|k}) + C_{i|k}(x_i - \bar{x}_{i|k}) + \psi_h(x_i, \bar{x}_{i|k}) + v_i = C_{i|k}x_i + \tau_{i|k} + \psi_h(x_i, \bar{x}_{i|k}) + v_i, \end{aligned} \quad (21)$$

following the linearization performed in (6), where $\mu_{i|k}$ and $\tau_{i|k}$ are defined in (7), $\psi_f(x_i, \bar{x}_{i|k}, u_{m,i})$ and $\psi_h(x_i, \bar{x}_{i|k})$ represent the linearization errors

$$\begin{aligned} \psi_f(x_i, \bar{x}_{i|k}, u_{m,i}) &= f(x_i, u_{m,i}) - f(\bar{x}_{i|k}, u_{m,i}) - A_{i|k}(x_i - \bar{x}_{i|k}), \\ \psi_h(x_i, \bar{x}_{i|k}) &= h(x_i) - h(\bar{x}_{i|k}) - C_{i|k}(x_i - \bar{x}_{i|k}). \end{aligned} \quad (22)$$

Prepared using rncauth.cls
DOI: 10.1002/rnc

Using $A_{i|k}$ and $C_{i|k}$, define $\mathcal{F}_k^o$ and $\mathcal{G}_k^o$ similarly to $\mathcal{F}_k$ and $\mathcal{G}_k$ in (9), respectively. Let $\eta_{f,k|k}^{k-N}$ and $\eta_{h,k|k}^{k-N}$ represent

$$\eta_{f,k|k}^{k-N} = \begin{bmatrix} \psi_f(x_{k-N}, \bar{x}_{k-N|k}, u_{m,k-N}) \\ \psi_f(x_{k-N+1}, \bar{x}_{k-N+1|k}, u_{m,k-N+1}) \\ \vdots \\ \psi_f(x_k, \bar{x}_{k|k}, u_{m,k}) \end{bmatrix}, \ \eta_{h,k|k}^{k-N} = \begin{bmatrix} \psi_h(x_{k-N}, \bar{x}_{k-N|k}) \\ \psi_h(x_{k-N+1}, \bar{x}_{k-N+1|k}) \\ \vdots \\ \psi_h(x_k, \bar{x}_{k|k}) \end{bmatrix}, \tag{23}$$

respectively. It then follows from (21) that $y_{m,k}^{k-N}$ can be expressed by

$$y_{m,k}^{k-N} = \mathcal{F}_k^o x_{k-N} + \mathcal{G}_k^o(\mu_{k|k}^{k-N} + \eta_{f,k|k}^{k-N} + w_k^{k-N}) + \tau_{k|k}^{k-N} + \eta_{h,k|k}^{k-N} + v_k^{k-N}. \tag{24}$$

With $\mathcal{H}_k\mathcal{F}_k^o = \mathcal{F}_k$ and $\mathcal{H}_k\mathcal{G}_k^o = \mathcal{G}_k$ (see the proof in Appendix I), substituting (24) into (8) gives

$$\sigma_k = \mathcal{F}_k x_{k-N} + \mathcal{G}_k(\eta_{f,k|k}^{k-N} + w_k^{k-N}) + \mathcal{H}_k(\eta_{h,k|k}^{k-N} + v_k^{k-N}). \tag{25}$$

Using (25), we further write (20) as

$$\begin{aligned} e_{k-N} = &\left[I - \alpha_k(M + \mathcal{F}_k^{\mathsf{T}}\bar{W}\mathcal{F}_k)^{-1}\mathcal{F}_k^{\mathsf{T}}\bar{W}\mathcal{F}_k\right](x_{k-N} - \bar{x}_{k-N|k}) \\ &- \alpha_k(M + \mathcal{F}_k^{\mathsf{T}}\bar{W}\mathcal{F}_k)^{-1}\mathcal{F}_k^{\mathsf{T}}\bar{W}\left[\mathcal{G}_k(\eta_{f,k|k}^{k-N} + w_k^{k-N}) + \mathcal{H}_k(\eta_{h,k|k}^{k-N} + v_k^{k-N})\right]. \end{aligned} \tag{26}$$

Since the a priori estimate $\bar{x}_{k-N|k}$ in Step (i) of Algorithm 1 is set to $\hat{x}_{k-N|k-1}^{\star}$, $x_{k-N} - \bar{x}_{k-N|k} = x_{k-N} - \hat{x}_{k-N|k-1}^{\star}$ is related to $e_{k-N-1} = x_{k-N-1} - \hat{x}_{k-N-1|k-1}^{\star}$ in forward prediction (Step (iii)) of Algorithm 1. This relation is expressed in (18), then (26) can be rearranged as

$$\begin{aligned} e_{k-N} &= \mathcal{A}_k e_{k-N-1} + \mathcal{B}_{w,k} w_k^{k-N-1} + \mathcal{B}_{v,k} v_k^{k-N-1} + \xi_k, \ k > N \\ e_0 &= \Gamma_N\left(x_0 - \bar{x}_{0|N}\right) + \mathcal{B}_{w,N} w_N^0 + \mathcal{B}_{v,N} v_N^0 + \xi_N \end{aligned} \tag{27}$$

where

$$\Gamma_k = I - \alpha_k(M + \mathcal{F}_k^{\mathsf{T}}\bar{W}\mathcal{F}_k)^{-1}\mathcal{F}_k^{\mathsf{T}}\bar{W}\mathcal{F}_k, \ k \geq N \tag{28}$$

$$\mathcal{A}_k = \Gamma_k\hat{\Xi}_{k-N-1,k-1}, \ k > N \tag{29}$$

$$\mathcal{B}_{w,k} = \begin{cases} -\alpha_k(M + \mathcal{F}_k^{\mathsf{T}}\bar{W}\mathcal{F}_k)^{-1}\mathcal{F}_k^{\mathsf{T}}\bar{W}\mathcal{G}_k, & k = N \\ \begin{bmatrix}\Gamma_k & -\alpha_k(M + \mathcal{F}_k^{\mathsf{T}}\bar{W}\mathcal{F}_k)^{-1}\mathcal{F}_k^{\mathsf{T}}\bar{W}\mathcal{G}_k\end{bmatrix}, & k > N \end{cases} \tag{30}$$

$$\mathcal{B}_{v,k} = \begin{cases} -\alpha_k(M + \mathcal{F}_k^{\mathsf{T}}\bar{W}\mathcal{F}_k)^{-1}\mathcal{F}_k^{\mathsf{T}}\bar{W}\mathcal{H}_k, & k = N \\ \begin{bmatrix}-\Gamma_k L & -\alpha_k(M + \mathcal{F}_k^{\mathsf{T}}\bar{W}\mathcal{F}_k)^{-1}\mathcal{F}_k^{\mathsf{T}}\bar{W}\mathcal{H}_k\end{bmatrix}, & k > N \end{cases} \tag{31}$$

$$\xi_k = -\alpha_k(M + \mathcal{F}_k^{\mathsf{T}}\bar{W}\mathcal{F}_k)^{-1}\mathcal{F}_k^{\mathsf{T}}\bar{W}\left(\mathcal{G}_k\eta_{f,k|k}^{k-N} + \mathcal{H}_k\eta_{h,k|k}^{k-N}\right), \ k \geq N \tag{32}$$

4.2. Bounds on linearization errors

The error dynamics (27) still cannot provide a direct insight about stability, because the linearization errors included in $\eta_{f,k|k}^{k-N}$ and $\eta_{h,k|k}^{k-N}$ in (23) are presented in ξ_k in (27). To address this issue, the

DOI: 10.1002/rnc

bounds on $\eta_{f,k|k}^{k-N}$ and $\eta_{h,k|k}^{k-N}$ are derived in this subsection. For this purpose, it is assumed that the nonlinearities in linearization errors $\psi_f(x_i, \bar{x}_{i|k}, u_{m,i})$ and $\psi_h(x_i, \bar{x}_{i|k})$ in (22) are bounded, as stated in the following assumption.

Assumption 3 [42]. There are positive real numbers κ_f, κ_h, and ε such that

$$\left\|\psi_f(x_i, \bar{x}_{i|k}, u_{m,i})\right\| \leq \kappa_f \left\|x_i - \bar{x}_{i|k}\right\|^2 \text{ and } \left\|\psi_h(x_i, \bar{x}_{i|k})\right\| \leq \kappa_h \left\|x_i - \bar{x}_{i|k}\right\|^2$$

hold for $x_i \in \mathbb{X}$, $u_{m,i} \in \mathbb{U}$ and $\left\|x_i - \bar{x}_{i|k}\right\| \leq \varepsilon$.

Let $r_w = \max_{w_i \in \mathbb{W}} \|w_i\|$ and $r_v = \max_{v_i \in \mathbb{V}} \|v_i\|$ denote the bounds of the disturbances w_i and the noises v_i over the compact sets $\mathbb{W}$ and $\mathbb{V}$, respectively. It follows from (23) and Assumption 3 that

$$\begin{aligned}\left\|\eta_{s,k|k}^{k-N}\right\| &\leq \kappa_s \left\| \begin{bmatrix} \left\|x_{k-N} - \bar{x}_{k-N|k}\right\|^2 \\ \left\|x_{k-N+1} - \bar{x}_{k-N+1|k}\right\|^2 \\ \vdots \\ \left\|x_k - \bar{x}_{k|k}\right\|^2 \end{bmatrix} \right\| \leq \kappa_s \varepsilon \left\| \begin{bmatrix} \left\|x_{k-N} - \bar{x}_{k-N|k}\right\| \\ \left\|x_{k-N+1} - \bar{x}_{k-N+1|k}\right\| \\ \vdots \\ \left\|x_k - \bar{x}_{k|k}\right\| \end{bmatrix} \right\| \\ &= \kappa_s \varepsilon \left\| \begin{bmatrix} x_{k-N} - \bar{x}_{k-N|k} \\ x_{k-N+1} - \bar{x}_{k-N+1|k} \\ \vdots \\ x_k - \bar{x}_{k|k} \end{bmatrix} \right\|, \ s \text{ represents } f \text{ or } h. \end{aligned} \tag{33}$$

With $x_{k-N} - \bar{x}_{k-N|k} = x_{k-N} - \hat{x}^{\star}_{k-N|k-1}$, the stacked vector of errors of pre-estimated states in the above equation can be further expressed by $e_{k-N-1} = x_{k-N-1} - \hat{x}^{\star}_{k-N-1|k-1}$ using (17) and (18):

$$\begin{aligned} \begin{bmatrix} x_{k-N} - \bar{x}_{k-N|k} \\ x_{k-N+1} - \bar{x}_{k-N+1|k} \\ \vdots \\ x_k - \bar{x}_{k|k} \end{bmatrix} &= \bar{\mathcal{F}}_k (x_{k-N} - \bar{x}_{k-N|k}) + \bar{\mathcal{G}}_k w_k^{k-N} + \bar{\mathcal{H}}_k v_k^{k-N} \\ &= \bar{\mathcal{F}}_k (x_{k-N} - \hat{x}^{\star}_{k-N|k-1}) + \bar{\mathcal{G}}_k w_k^{k-N} + \bar{\mathcal{H}}_k v_k^{k-N} \\ &= \hat{\mathcal{F}}_k e_{k-N-1} + \hat{\mathcal{G}}_k \begin{bmatrix} w_{k-N-1} \\ w_k^{k-N} \end{bmatrix} + \hat{\mathcal{H}}_k \begin{bmatrix} v_{k-N-1} \\ v_k^{k-N} \end{bmatrix}, \end{aligned} \tag{34}$$

where $\bar{\mathcal{F}}_k$, $\bar{\mathcal{G}}_k$, and $\bar{\mathcal{H}}_k$ are defined based on (17), similarly to $\mathcal{F}_k$, $\mathcal{G}_k$, and $\mathcal{H}_k$ in (9). The last equation in (34) is obtained from (18), with $\hat{\mathcal{F}}_k$, $\hat{\mathcal{G}}_k$, and $\hat{\mathcal{H}}_k$ defined as

$$\hat{\mathcal{F}}_k = \bar{\mathcal{F}}_k \hat{\Xi}_{k-N,k-1}, \ \hat{\mathcal{G}}_k = \begin{bmatrix} \bar{\mathcal{F}}_k & \bar{\mathcal{G}}_k \end{bmatrix}, \ \hat{\mathcal{H}}_k = \begin{bmatrix} -\bar{\mathcal{F}}_k L & \bar{\mathcal{H}}_k \end{bmatrix}.$$

Therefore, the upper bounds of $\left\|\eta_{f,k|k}^{k-N}\right\|$ and $\left\|\eta_{h,k|k}^{k-N}\right\|$ can be expressed by

$$\left\|\eta_{s,k|k}^{k-N}\right\| \leq \kappa_s \varepsilon \left(\varrho_e \left\|e_{k-N-1}\right\| + \varrho_w \sqrt{N+2} r_w + \varrho_v \sqrt{N+2} r_v\right), \ s \text{ represents } f \text{ or } h, \tag{35}$$

according to (33) and (34), where the positive scalars ϱ_e, ϱ_w, and ϱ_v are larger than or equal to the maximum singular values of $\hat{\mathcal{F}}_k$, $\hat{\mathcal{G}}_k$, and $\hat{\mathcal{H}}_k$ at all time instants, respectively.

Prepared using rncauth.cls
DOI: 10.1002/rnc

4.3. Error bounds of state estimates

Considering the bounds of linearization errors in (35), further insights about the error dynamics (27) are developed in this subsection by deriving a time-varying bounding sequence for the estimation errors.

For a generic matrix X, let $\bar{\sigma}(X)$ and $\underline{\sigma}(X)$ represent its maximum and minimum singular values, respectively. Then, we define

$$\begin{aligned} &\delta_\Gamma = \max_k \bar{\sigma}(\Gamma_k),\ \delta_\mathcal{F} = \max_k \bar{\sigma}(\mathcal{F}_k),\ \delta_\mathcal{G} = \max_k \bar{\sigma}(\mathcal{G}_k),\ \delta_\mathcal{H} = \max_k \bar{\sigma}(\mathcal{H}_k),\ \delta_W = \bar{\sigma}(\bar{W}), \\ &\delta_L = \bar{\sigma}(L), \delta_\Xi = \max_k \bar{\sigma}(\hat{\Xi}_{k-N-1,k-1}),\ \mu_M = \underline{\sigma}(M),\ \mu_O = \min_k \underline{\sigma}(\mathcal{F}_k^\mathsf{T} \bar{W} \mathcal{F}_k). \end{aligned} \tag{36}$$

From the step length $\alpha_k \in (0, 1]$ and the definitions (30) and (31), the upper bounds for $\left\|\mathcal{B}_{w,k} w_k^{k-N-1}\right\|$ and $\left\|\mathcal{B}_{v,k} v_k^{k-N-1}\right\|$ are derived as

$$\begin{aligned} \left\|\mathcal{B}_{w,k} w_k^{k-N-1}\right\| &\le \|\Gamma_k w_{k-N-1}\| + \left\|\alpha_k (M + \mathcal{F}_k^\mathsf{T} \bar{W} \mathcal{F}_k)^{-1} \mathcal{F}_k^\mathsf{T} \bar{W} \mathcal{G}_k w_k^{k-N}\right\| \\ &\le \delta_\Gamma r_w + \frac{\delta_\mathcal{F} \delta_W \delta_\mathcal{G}}{\mu_M + \mu_O} \sqrt{N+1}\, r_w, \end{aligned} \tag{37}$$

$$\begin{aligned} \left\|\mathcal{B}_{v,k} v_k^{k-N-1}\right\| &\le \|\Gamma_k L v_{k-N-1}\| + \left\|\alpha_k (M + \mathcal{F}_k^\mathsf{T} \bar{W} \mathcal{F}_k)^{-1} \mathcal{F}_k^\mathsf{T} \bar{W} \mathcal{H}_k v_k^{k-N}\right\| \\ &\le \delta_\Gamma \delta_L r_v + \frac{\delta_\mathcal{F} \delta_W \delta_\mathcal{H}}{\mu_M + \mu_O} \sqrt{N+1}\, r_v, \end{aligned} \tag{38}$$

respectively, for $k > N$. When $k = N$, the bounds on $\left\|\mathcal{B}_{w,k} w_k^{k-N}\right\|$ and $\left\|\mathcal{B}_{v,k} v_k^{k-N}\right\|$ are actually the second term on the right-hand side of (37) and (38), respectively. Following (32) and (35), the upper bound for $\|\xi_k\|$ is

$$\begin{aligned} \|\xi_k\| &\le \frac{\delta_\mathcal{F} \delta_W}{\mu_M + \mu_O} \left(\delta_\mathcal{G} \left\|\eta_{f,k|k}^{k-N}\right\| + \delta_\mathcal{H} \left\|\eta_{h,k|k}^{k-N}\right\| \right) \\ &= \frac{\delta_\mathcal{F} \delta_W \varepsilon (\delta_\mathcal{G} \kappa_f + \delta_\mathcal{H} \kappa_h)}{\mu_M + \mu_O} \left(\varrho_e \|e_{k-N-1}\| + \varrho_w \sqrt{N+2}\, r_w + \varrho_v \sqrt{N+2}\, r_v \right). \end{aligned} \tag{39}$$

Theorem 1

For $k > N$, the norm of the estimation error is upper bounded as $\|e_{k-N}\| \le \zeta_{k-N}$, where $\{\zeta_k\}$ is a sequence generated by

$$\zeta_k = a\zeta_{k-1} + b,\ k = 1, 2, \cdots \tag{40}$$

with

$$\begin{aligned} a &= \delta_\Gamma \delta_\Xi + \frac{\delta_\mathcal{F} \delta_W \varepsilon \varrho_e (\delta_\mathcal{G} \kappa_f + \delta_\mathcal{H} \kappa_h)}{\mu_M + \mu_O}, \\ b &= \left(\delta_\Gamma + \frac{\delta_\mathcal{F} \delta_W \delta_\mathcal{G}}{\mu_M + \mu_O} \sqrt{N+1} + \frac{\delta_\mathcal{F} \delta_W \varepsilon \varrho_w (\delta_\mathcal{G} \kappa_f + \delta_\mathcal{H} \kappa_h)}{\mu_M + \mu_O} \sqrt{N+2} \right) r_w \\ &\quad + \left(\delta_\Gamma \delta_L + \frac{\delta_\mathcal{F} \delta_W \delta_\mathcal{H}}{\mu_M + \mu_O} \sqrt{N+1} + \frac{\delta_\mathcal{F} \delta_W \varepsilon \varrho_v (\delta_\mathcal{G} \kappa_f + \delta_\mathcal{H} \kappa_h)}{\mu_M + \mu_O} \sqrt{N+2} \right) r_v. \end{aligned} \tag{41}$$

Furthermore, if the weighting matrices M and W are selected such that $a < 1$, the bounding sequence $\{\zeta_k\}$ has the following properties:

DOI: 10.1002/rnc

(i) $\{\zeta_k\}$ converges exponentially to $\zeta_\infty = \frac{b}{1-a}$;

(ii) if $\zeta > \zeta_\infty$, then $\zeta_{k+1} < \zeta_k$.

Proof

The theorem can be proven by showing $\|e_{i+1}\| \leq a\,\|e_i\| + b \leq a\zeta_i + b = \zeta_{i+1}$ when assuming $\|e_i\| \leq \zeta_i$, according to (27)-(32) and (37)-(39). The proof of the property (ii) follows the proof of Theorem 3 in [35]. □

The two properties in Theorem 1 determine the boundedness of the state estimation errors given by the proposed real-time MHO-PE. Since $\delta_\Gamma < 1$ according to (28), a sufficient condition for $a < 1$ is

$$\delta_\Xi + \frac{\delta_\mathcal{F}\delta_W\varepsilon\varrho_e(\delta_\mathcal{G}\kappa_f + \delta_\mathcal{H}\kappa_h)}{\mu_M + \mu_O} < 1. \tag{42}$$

Note that $\delta_\Xi < 1$ due to the use of the pre-stabilizing Luenberger observer. Therefore, the bounding sequence converges exponentially if the weighting matrix M is selected such that

$$\mu_M > \frac{\delta_\mathcal{F}\delta_W\varepsilon\varrho_e(\delta_\mathcal{G}\kappa_f + \delta_\mathcal{H}\kappa_h)}{1 - \delta_\Xi} - \mu_O. \tag{43}$$

The above derivation is attributed to the second term in (41) which describes the effect of linearization errors in the real-time iteration scheme. In contrast, when the optimization at each time instant k is fully solved without the real-time restriction, the optimality condition can be used to derive the error dynamics, as in [33] for the MHO formulation (3). Therein, no linearization errors was introduced, thus the second term in the definition (41) would not present. As a result, in [33], an arbitrary choice of the weighting matrix M can ensure stability of the state estimation error dynamics if $\delta_\Xi < 1$ holds. This comparison shows that the fixed number of iterations required in the real-time implementation indeed need to be accounted for to ensure boundedness of the state estimation errors.

For the proposed real-time MHO-PE described in Section 3, the tuning parameters include the pre-estimating observer gain L, and the weighting matrices M and W. Below we describe the tuning guidelines revealed by the above analysis:

- As in Kalman filtering, W corresponds to the inverse of the measurement noise covariance or the beliefs in sensor measurements.
- The selection of the observer gain L is independent from W. By following any nonlinear Luenberger observer design such as in [39], L is selected so that the error dynamics of the pre-estimating observer is stabilized and achieves a large decay rate. The larger the decay rate of the error dynamics is, the less error accumulation would be along the prediction horizon.
- The choice of M should satisfy (43), and it leads to trade-offs between stability and estimation errors. According to the MHO-PE formulation (4), as M increases to ensure (43), the proposed MHO-PE behaves closer to the stabilized pre-estimating observer, hence the convergence

DOI: 10.1002/rnc

of the bounding error sequence improves. Meanwhile, the weights on the output estimation errors in the objective function relatively decrease, thus the online optimization plays less significant role and estimation errors may increase.

The selections of W and L affect the available choices of M, since they determine the value of the right-hand side of (43). First, the observer gain L should be stabilizing, so that $\delta_{\Xi} < 1$ is ensured, and an explicit condition (43) can be derived for selecting M. Otherwise, we might have $\delta_{\Xi} \geq 1$, and no useful condition for selecting M could be obtained from (42). Second, if the observer error dynamics achieves a larger decay rate by choosing L, then δ_{Ξ} is smaller, and the right-hand side of (43) also decreases, hence an M with a smaller μ_M is allowed by (43). By choosing such an M, the second term in the objective function (4) has a relatively larger weight than the first term, which enforces the state estimation errors to decrease.

5. SIMULATION STUDY

In this section, we focus on an aircraft application where it is of great importance to 1) detect AOA sensor faults; and 2) provide reliable AOA estimates after total loss of AOA sensors. In our proposed approach, AOA estimates are computed from other measurable signals by exploiting a low-order aerodynamic-independent model as explained in Section 5.1. The discrepancy between AOA estimates and AOA sensor outputs are used to indicate the occurrence of sensor faults. The estimates replace AOA sensor outputs after all available AOA sensors are indicated as faulty.

5.1. Aerodynamic-independent model

The RECONFIGURE project focuses on the longitudinal motion of an aircraft [1]. Thus the following longitudinal model is derived for AOA sensor fault detection and estimation:

$$\begin{cases} \dot{x}(t) = g\left(x(t), u_m(t) - w(t)\right) \\ y_m(t) = h(x(t)) + v(t) \end{cases} \tag{44}$$

where the system states $x \in \mathbb{R}^{n_x}$, the measured system inputs $u_m \in \mathbb{R}^{n_u}$, and the measured outputs $y_m \in \mathbb{R}^{n_y}$ are defined as

$$x = \begin{bmatrix} \alpha & V_t & \theta \end{bmatrix}^{\mathsf{T}}, \; u_m = \begin{bmatrix} A_{xm} & A_{zm} & q_m \end{bmatrix}^{\mathsf{T}} = \begin{bmatrix} A_x + w_{A_x} & A_z + w_{A_z} & q + w_q \end{bmatrix}^{\mathsf{T}},$$
$$y_m = \begin{bmatrix} V_{tm} & V_{zm} & \theta_m \end{bmatrix}^{\mathsf{T}} = \begin{bmatrix} V_t + v_{V_t} & V_z + v_{V_z} & \theta + v_\theta \end{bmatrix}^{\mathsf{T}},$$

with angle-of-attack α (rad), true airspeed V_t (kts), pitch angle θ (rad), horizontal load factor A_x (kt/s^2), vertical load factor A_z (kt/s^2), pitch rate q (rad/s), and vertical speed V_z (kts). In (44), $w = \begin{bmatrix} w_{A_x} & w_{A_z} & w_q \end{bmatrix}^{\mathsf{T}}$ and $v = \begin{bmatrix} v_{V_t} & v_{V_z} & v_\theta \end{bmatrix}^{\mathsf{T}}$ represent the measurement noises of system

Prepared using rncauth.cls
DOI: 10.1002/rnc

inputs and outputs, respectively. The detailed dynamic and output equations in (44) are as follows:

$$\begin{aligned}
\dot{\alpha} &= \frac{1}{V_t}\{-(A_{xm}-w_{A_x})\sin\alpha+(A_{zm}-w_{A_z})\cos\alpha+g\cos(\alpha-\theta)\}+q_m-w_q,\\
\dot{V}_t &= (A_{xm}-w_{A_x})\cos\alpha+(A_{zm}-w_{A_z})\sin\alpha+g\sin(\alpha-\theta),\\
\dot{\theta} &= q_m-w_q,\\
V_{tm} &= V_t+v_{V_t},\ V_{zm}=-V_t\sin(\alpha-\theta)+v_{V_z},\ \theta_m=\theta+v_\theta.
\end{aligned}$$

Note that the above model includes no aerodynamic parameters, thus is independent of aircraft and flight envelope [8, 43]. This feature avoids the issue of robustness to uncertain aerodynamic parameters.

To deal with sampled measurements, the following approximated discrete-time model is derived from (44) by applying the Euler method in numerical integration:

$$\begin{aligned}
x_{k+1} &= f(x_k,u_{m,k})+w_k = x_k+t_s g\left(x_k,u_{m,k}\right)+w_k\\
y_{m,k} &= h(x_k)+v_k,
\end{aligned}$$

where t_s represents the sampling interval, and w_k accounts for both measurement noises of $u_{m,k}$ and the numerical integration errors.

5.2. *Comparative simulation results*

The results of a comparative simulation study are presented using data generated from the RECONFIGURE benchmark simulator [1]. The sampling interval is 0.08 s. The standard deviations of measurement noises are listed in Table I. Two challenging flight scenarios as shown in Figure 2 are chosen to test the performance of different algorithms. In both scenarios, the AOA α, altitude h, and vertical load factor A_z of the aircraft change significantly.

Table I. Standard deviations of measurement noises in measured inputs and outputs

A_{xm}	A_{zm}	q_m	V_{tm}	V_{zm}	θ_m
0.3215 kt/s^2	0.3215 kt/s^2	0.0140 rad/s	0.7775 kts	0.5832 kts	0.0017 rad

The EKF and real-time algorithms for the three MHO formulations are compared in terms of computational cost and performance when applied to the AOA sensor fault detection and estimation problem. In order to perform a fair comparison, the weighting matrices in the three MHO formulations are the same, i.e., $M=\text{diag}(131.31, 0.04, 131.31)$, $Q=\text{diag}(8.01, 1.41, 8.01)\times 10^5$, $W=\text{diag}(1.65, 2.94, 3.28\times 10^5)$, while Q^{-1} and W^{-1} are chosen as the covariances of process noises and measurement noises in EKF. For the sake of brevity, the MHO formulations (2) and (3) are referred to as MHO-wD (with disturbances) and MHO-woD (without disturbances) in the rest of this section, respectively.

Prepared using rncauth.cls
DOI: 10.1002/rnc

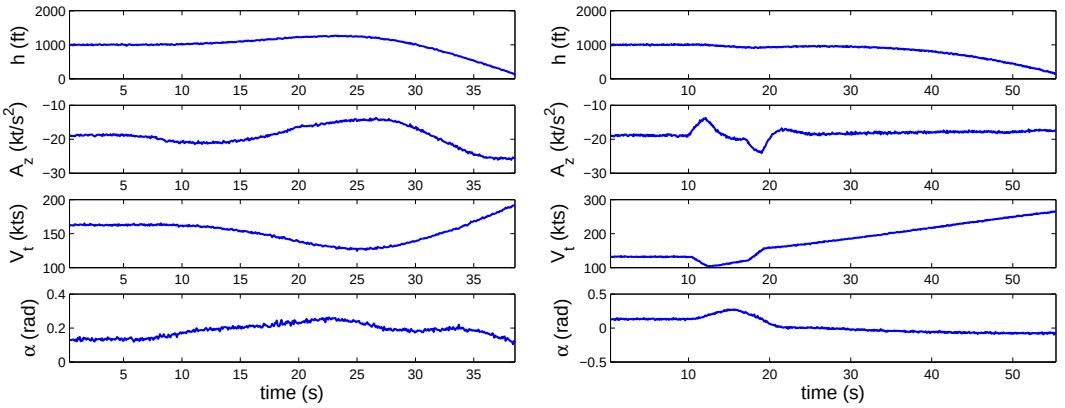

(a) Scenario 1. (b) Scenario 2.

Figure 2. Flight data in two test scenarios.

With a short horizon length $N = 2$, the AOA estimates of different MHOs as well as EKF are depicted in Figure 3. It can be seen that EKF gives the worst performance in both scenarios, while the AOA estimates of all the three real-time MHO algorithms are almost the same. When increasing the horizon length to $N = 15$, the MHO-woD performs even worse than EKF, as illustrated in Figure 4. This is due to the error propagation of the open-loop forward prediction adopted in the MHO-woD formulation (3), which becomes more severe when the horizon length increases. By looking further into spectral radius of the linearized dynamics of each iteration per sample as depicted in Figure 5, it can be found that the linearized dynamics in the MHO-woD iterations are unstable or marginally stable, hence the errors get amplified in the open-loop forward prediction. In contrast, the linearized dynamics in the MHO-PE iterations are asymptotically stable thanks to the use of a pre-estimating observer.

Figure 6 further shows how the performance of real-time MHO algorithms varies with different horizon lengths. As expected, both the root mean square error and the absolute error of MHO-woD estimates increase with the increased horizon length, and its performance eventually becomes worse than EKF. Although the MHO-PE neglects process disturbances as the MHO-woD does, a pre-estimating observer is exploited in the MHO-PE to attenuate the error propagation in its closed-loop forward prediction. Therefore, the estimation errors of the MHO-PE are always smaller than EKF, and converge with the increased horizon length. Because of explicitly accounting for process disturbances, the MHO-wD achieves the best performance at the cost of larger computational burden. In all the three real-time MHO algorithms, the increase of horizon length may not lead to reduced estimation errors. As can be seen in Figure 6, the maximum absolute errors of estimates slowly grow with the increasing horizon length. Since each maximum absolute error corresponds to the worst-case scenario during a single simulation run, the above phenomenon is consistent with

Prepared using rncauth.cls
DOI: 10.1002/rnc

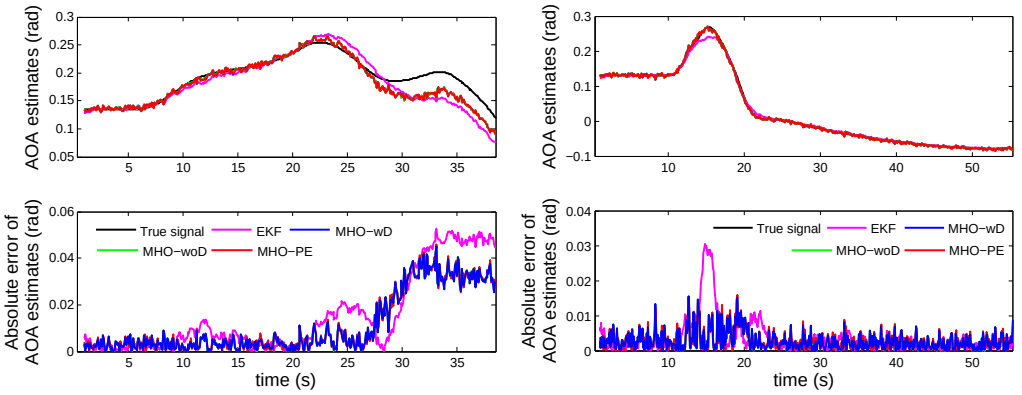

(a) Scenario 1. (b) Scenario 2.

Figure 3. AOA estimates with the horizon length $N = 2$.

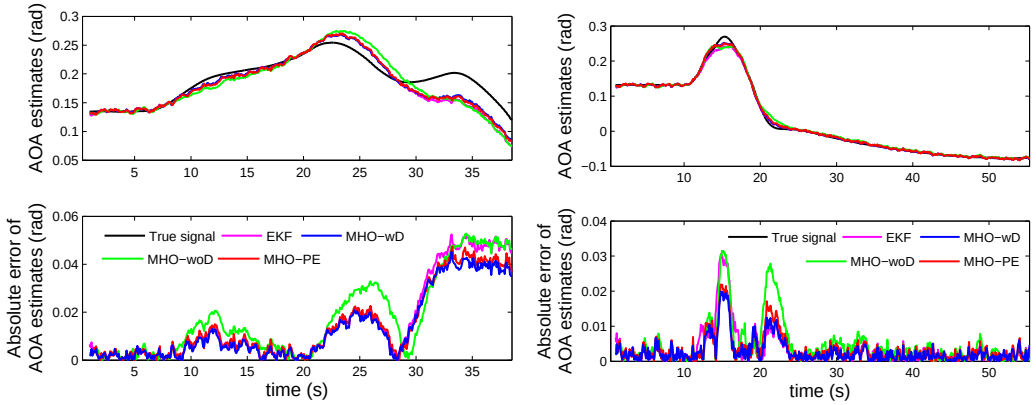

(a) Scenario 1. (b) Scenario 2.

Figure 4. AOA estimates with the horizon length $N = 15$.

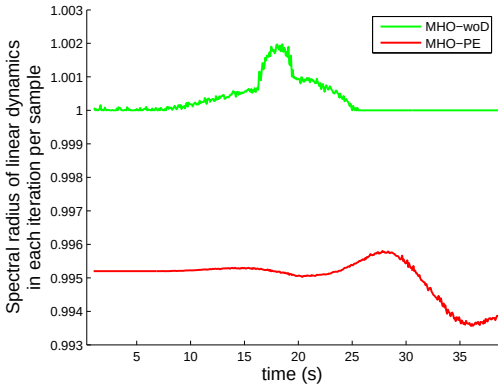

Figure 5. Spectral radius of linearized dynamics in each iteration per sample in Scenario 1.

Prepared using rncauth.cls
DOI: 10.1002/rnc

the worst-case error bound $\zeta_\infty = \frac{b}{1-a}$ given in Theorem 1, where b monotonically grows with the horizon length according to its definition. Besides the horizon length, the size of the estimation error bound is related to the weighting matrices in the objective function. Even for linear systems, minimizing the worst-case error bound by systematically tuning the weighting matrices leads to a non-convex optimization problem [35]. It is a future research challenge for our nonlinear MHO-PE with the proposed real-time iteration scheme, although some heuristic tuning guidelines are provided at the end of Section 4.3.

For the three real-time MHO algorithms, their worst-case and average computation time per sample using different horizon lengths is reported in Figure 7. All three algorithms are implemented in a MATLAB environment, on a computer with 2.5 GHz process and 6 GB RAM. It can be seen that the MHO-wD is the most expensive in computation, while the MHO-woD and MHO-PE can be much more computationally efficient, especially when the horizon is long. In summary, considering the computational cost in the MHO-wD and the error accumulation in the MHO-woD, the MHO-PE achieves a good balance between computational efficiency and performance.

It is straightforward to use the discrepancy between the AOA estimates $\hat{\alpha}_k$ and the AOA sensor outputs $\alpha_{m,k}$, i.e., $r_k = \alpha_{m,k} - \hat{\alpha}_k$, to indicate the occurrence of sensor faults. The size of this residual signal is evaluated by its root mean square value over a sliding window $[k - N_e, k]$. With a horizon length $N = 4$, an evaluation sliding window length $N_e = 20$, and a detection threshold 0.0454, the fault detection results of the MHO-PE in the presence of runaway, oscillation, and bias fault signals are illustrated in Figure 8.

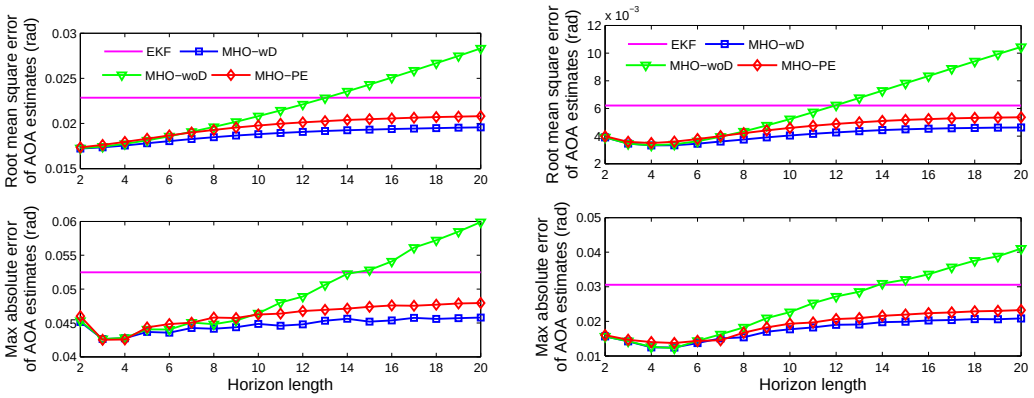

(a) Scenario 1. (b) Scenario 2.

Figure 6. AOA estimation errors with different horizon lengths.

Prepared using rncauth.cls
DOI: 10.1002/rnc

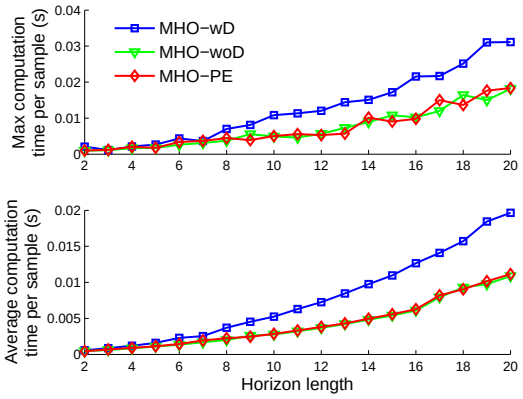

Figure 7. Computation time per sample using different horizon length.

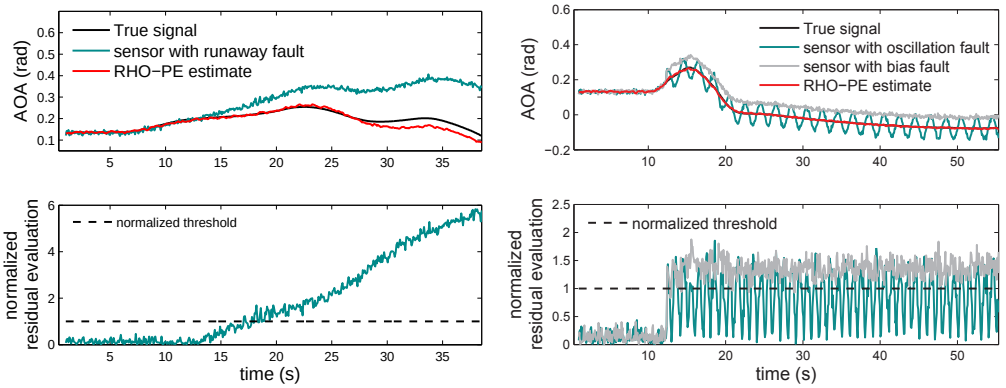

(a) Scenario 1. (b) Scenario 2.

Figure 8. fault detection results of the MHO-PE in the presence of runaway, oscillation, and bias faults.

6. CONCLUSIONS

This paper has presented a real-time moving horizon observer with pre-estimation. The use of a pre-estimating observer replaces explicit disturbance estimates that compensate for model uncertainties in forward prediction. This strategy significantly reduces the computational complexity by avoiding the calculation of disturbance estimates during the online optimization. A real-time iteration scheme with one iteration of sequential quadratic programming per sample is performed to achieve real-time implementability. Stability analysis of the estimation error dynamics is derived to provide useful insights about parameter tuning for trade-offs between stability and estimation performance. Simulation studies using a nonlinear passenger aircraft benchmark simulator have been presented. The results validate the promising performance of the proposed approach, and highlight its real-time applicability, compared to extended Kalman filtering and two other moving horizon observers.

Prepared using rncauth.cls
DOI: 10.1002/rnc

APPENDIX

I. PROOF FOR $\mathcal{H}_k\mathcal{F}_k^o = \mathcal{F}_k$ AND $\mathcal{H}_k\mathcal{G}_k^o = \mathcal{G}_k$

For $1 \le i \le N+1$, let $\mathcal{H}_{k,i} = \begin{bmatrix} H_{k,i,1} & H_{k,i,2} & \cdots & H_{k,i,i} & 0 & \cdots & 0 \end{bmatrix}$, $F_{k,i}$, and $F_{k,i}^o$ denote the ith block-row of $\mathcal{H}_k$, $\mathcal{F}_k$ and $\mathcal{F}_k^o$, respectively. Since $\mathcal{H}_k$ and $\mathcal{F}_k$ are defined in (9) and $\mathcal{F}_k^o$ is defined similarly to $\mathcal{F}_k$ using $A_{i|k}$ and $C_{i|k}$ in (21), their block entries $H_{k,i,j}$, $F_{k,i}$, and $F_{k,i}^o$ in the ith block-row are defined as

$$H_{k,i,j} = \begin{cases} I & j = i,\ 1 \le i \le N+1 \\ -C_{k-N+i-1|k}L & j = i-1,\ 2 \le i \le N+1 \\ -C_{k-N+i-1|k}\prod_{m=k-N+j}^{k-N+i-2}\Phi_{m|k}L & 1 \le j \le i-2,\ 3 \le i \le N+1 \end{cases},$$

$$F_{k,i} = \begin{cases} C_{k-N+i-1|k} & i = 1 \\ C_{k-N+i-1|k}\prod_{m=k-N}^{k-N+i-2}\Phi_{m|k} & 2 \le i \le N+1 \end{cases},$$

$$F_{i|k}^o = \begin{cases} C_{k-N+i-1|k} & i = 1 \\ C_{k-N+i-1|k}\prod_{m=k-N}^{k-N+i-2}A_{m|k} & 2 \le i \le N \end{cases}.$$

With the above notations, $\mathcal{H}_k\mathcal{F}_k^o = \mathcal{F}_k$ can be proven by showing

$$\sum_{j=1}^{i} H_{k,i,j}F_{k,j}^o = F_{k,i} \tag{45}$$

for $i = 1, \cdots, N+1$. This is obviously valid when $i = 1$. For $i = 2$ and $i = 3$, we have

$$\sum_{j=1}^{2} H_{k,2,j}F_{k,j}^o = -C_{k-N+1|k}LC_{k-N|k} + C_{k-N+1|k}A_{k-N|k} = C_{k-N+1|k}\Phi_{k-N|k} = F_{k,2}$$

$$\begin{aligned}\sum_{j=1}^{3} H_{k,3,j}F_{k,j}^o &= -C_{k-N+2|k}\Phi_{k-N+1|k}LC_{k-N|k} - C_{k-N+2|k}LC_{k-N+1|k}A_{k-N|k} \\ &\quad + C_{k-N+2|k}A_{k-N+1|k}A_{k-N|k} \\ &= -C_{k-N+2|k}\Phi_{k-N+1|k}LC_{k-N|k} + C_{k-N+2|k}\Phi_{k-N+1|k}A_{k-N|k} \\ &= C_{k-N+2|k}\Phi_{k-N+1|k}\Phi_{k-N|k} = F_{k,3}.\end{aligned}$$

The same procedure can be easily extended to the cases with $i > 3$, leading to our claim $\mathcal{H}_k\mathcal{F}_k^o = \mathcal{F}_k$. The proof of $\mathcal{H}_k\mathcal{G}_k^o = \mathcal{G}_k$ directly follows the above idea, thus is omitted.

REFERENCES

1. Goupil P, Boada-Bauxell J, Marcos A, Rosa P, Kerr M, Dalbies L. An overview of the FP7 RECONFIGURE project: industrial, scientific and technological objectives. *Proceedings of 9th IFAC Symposium on Safeprocess*, Paris, France, 2015; 976–981.

Prepared using rncauth.cls
DOI: 10.1002/rnc

2. Marzat J, Piet-Lahanier H, Damongeot F, Walter E. Model-based fault diagnosis for aerospace systems: a survey. *Proceedings of the Institution of Mechanical Engineering, Part G: Journal of Aerospace Engineering* 2012; **226**(10):1329–1360.
3. Castaldi P, Geri W, Bonfè M, Simani S, Benini M. Design of residual generators and adaptive filters for the FDI of aircraft model sensors. *Control Engineering Practice* 2010; **18**(5):449–459.
4. Besançon G. High-gain observation with disturbance attenuation and application to robust fault detection. *Automatica* 2003; **39**:1095–1102.
5. Hammouri H, Kinnaert M, Yaagoubi EHE. Observer-based approach to fault detection and isolation for nonlinear systems. *IEEE Transactions on Automatic Control* 1999; **44**(10):1879–1884.
6. Shtessel Y, Edwards C, Fridman L, Levant A. *Sliding mode control and observation*. Springer, 2014.
7. Yan XG, Edwards C. Nonlinear robust fault reconstruction and estimation using a sliding mode observer. *Automatica* 2007; **43**(9):1605–1614.
8. Van Eykeren L, Chu QP. Sensor fault detection and isolation for aircraft control systems by kinematic relations. *Control Engineering Practice* 2014; **31**:200–210.
9. Gu Y, Gross J, Rhudy MB, Lassak K. A fault-tolerant multiple sensor fusion approach applied to UAV attitude estimation. *International Journal of Aerospace Engineering* 2016; Doi:10.1155/2016/6217428.
10. Hansen S, Blanke M. Diagnosis of airspeed measurement faults for unmanned aerial vehicles. *IEEE Transactions on Aerospace and Electronic Systems* 2014; **50**(1):224–239.
11. Lu P, van Kampen E, de Visser C, Chu Q. Nonlinear aircraft sensor fault reconstruction in the presence of disturbances validated by real flight data. *Control Engineering Practice* 2016; **49**:112–128.
12. Alwi H, Edwards C. Robust fault reconstruction for linear parameter varying systems using sliding mode observers. *International Journal of Robust and Nonlinear Control* 2014; **24**(14):1947–1968.
13. Alwi H, Edwards C. Development and application of sliding mode LPV fault reconstruction schemes for the ADDSAFE benchmark. *Control Engineering Practice* 2014; **31**:148–170.
14. Ossmann D, Joos H. Enhanced detection and isolation of angle of attack sensor faults. *Proceedings of the AIAA Guidance, Navigation, and Control Conference*, San Diego, California, 2016. Doi:10.2514/6.2016-1135.
15. Henry D, Cieslak J, Zolghadri A, Efimov D. H_∞/H_- LPV solutions for fault detection of aircraft actuator faults: Bridging the gap between theory and practice. *International Journal of Robust and Nonlinear Control* 2015; **25**(5):649–672.
16. Michalska H, Mayne DQ. Moving horizon observers and observer-based control. *IEEE Transactions on Automatic Control* 1995; **40**(6):995–1006.
17. Alamir M. Nonlinear moving horizon observers: Theory and real-time implementation. *Nonlinear Observers and Applications*. Springer, 2007; 139–179.
18. Rao CV, Rawlings JB, Mayne DQ. Constrained state estimation for nonlinear discrete-time systems: stability and moving horizon approximations. *IEEE Transactions on Automatic Control* 2003; **48**(2):246–257.
19. Rawlings JB, Bakshi BR. Particle filtering and moving horizon estimation. *Computers and Chemical Engineering* 2006; **30**(10-12):1529–1541.
20. Haseltine EL, Rawlings JB. Critical evaluation of extended kalman filtering and moving-horizon estimation. *Industrial & engineering chemistry research* 2005; **44**(8):2451–2460.
21. Diehl M, Ferreau HJ, Haverbeke N. Efficient numerical methods for nonlinear MPC and moving horizon estimation. *Nonlinear model predictive control*. Springer, 2009; 391–417.
22. Alessandri A, Gaggero M. Fast moving horizon state estimation for discrete-time systems using single and multi iteration descent methods. *IEEE Transactions on Automatic Control* 2017; doi:10.1109/TAC.2017.2660438.
23. Sui D, Johansen TA. Moving horizon observer with regularisation for detectable systems without persistence of excitation. *International Journal of Control* 2011; **84**(6):1041–1054.
24. Farina M, Ferrari-Trecate G, Scattolini R. Distributed moving horizon estimation for nonlinear constrained systems. *International Journal of Robust and Nonlinear Control* 2012; **22**(2):123–143.

Prepared using rncauth.cls
DOI: 10.1002/rnc

25. Johansen TA, Sui D, Nybø R. Regularized nonlinear moving-horizon observer with robustness to delayed and lost data. *IEEE Transactions on Control Systems Technology* 2013; **21**(6):2114–2128.
26. Geebelen K, Wagner A, Gros S, Swevers J, Diehl M. Moving horizon estimation with a Huber penalty function for robust pose estimation of tethered airplanes. *American Control Conference, 2013*, 2013; 6169–6174.
27. Legowo A, Okubo H, Muramatsu E, Tokutake H. Application of moving horizon method to states estimation from flight test data. *Transactions of the Japan Society for Aeronautical and Space Sciences* 2001; **44**(145):150–154.
28. Ohtsuka T, Fujii HA. Nonlinear receding-horizon state estimation by real-time optimization technique. *Journal of Guidance, Control, and Dynamics* 1996; **19**(4):863–870.
29. Polóni T, Rohal-Ilkiv B, Johansen TA. Moving horizon estimation for integrated navigation filtering. *Proceedings of 5th IFAC Conference on Nonlinear Model Predictive Control*, Seville, Spain, 2015; 519–526.
30. Vandersteen J, Diehl M, Aerts C, Swevers J. Spacecraft attitude estimation and sensor calibration using moving horizon estimation. *Journal of Guidance, Control, and Dynamics* 2013; **36**(3):734–742.
31. Haverbeke N. Efficient numerical methods for moving horizon estimation. Phd thesis, Katholieke Universiteit Leuven 2011.
32. Zavala VM, Laird CD, Biegler LT. A fast moving horizon estimation algorithm based on nonlinear programming sensitivity. *Journal of Process Control* 2008; **18**(9):876–884.
33. Alessandri A, Baglietto M, Battistelli G. Moving-horizon state estimation for nonlinear discrete-time systems: new stability results and approximation schemes. *Automatica* 2008; **44**:1753–1765.
34. Wynn A, Vukov M, Diehl M. Convergence guarantees for moving horizon estimation based on the real-time iteration scheme. *IEEE Transactions on Automatic Control* 2014; **59**(8):2215–2221.
35. Sui D, Johansen TA, Le F. Linear moving horizon estimation with pre-estimating observer. *IEEE Transactions on Automatic Control* 2010; **55**(10):2363–2368.
36. Sui D, Johansen TA. Linear constrained moving horizon estimator with pre-estimating observer. *Systems and Control Letters* 2014; **67**:40–45.
37. Polóni T, Eielsen AA, Johansen TA, *et al.*. Adaptive model estimation of vibration motion for a nanopositioner with moving horizon optimized extended kalman filter. *Journal of Dynamic Systems, Measurement, and Control* 2013; **135**(4):041 019.
38. Sunwantong R, Bertrand S, Dumur D, Beauvois D. Stability of a nonlinear moving horizon estimator with pre-estimation. *Proceedings of 2014 American Control Conference*, Portland, Oregon, 2014; 5688–5693.
39. Zemouche A, Boutayeb M. On LMI conditions to design observers for Lipschitz nonlinear systems. *Automatica* 2013; **49**:585–591.
40. Kang W. Moving horizon numerical observers of nonlinear control systems. *IEEE Transactions on Automatic Control* 2006; **51**(2):344–350.
41. Nocedal J, Wright SJ. *Numerical Optimization*. 2nd edn., Springer: New York, USA, 2006.
42. Reif K, Sonnemann F, Unbehauen R. An EKF-based nonlinear observer with a prescribed degree of stability. *Automatica* 1998; **34**(9):1119–1123.
43. Wan Y, Keviczky T, Verhaegen M. Robust air data sensor fault diagnosis with enhanced fault sensitivity using moving horizon estimation. *Proceedings of the 2016 American Control Conference*, Boston, 2016; 5969–5975.

DOI: 10.1002/rnc